

Formation of thin bifurcated current sheets by quasisteady compression

Karl Schindler¹ and Michael Hesse²

¹Ruhr University Bochum, 44780 Bochum, Germany

²NASA/Goddard Space Flight Center, Greenbelt, Maryland 20771, USA

(Received 18 January 2008; accepted 19 March 2008; published online 29 April 2008)

Thin current sheets with half-widths in the range of about 10 or less ion inertial lengths (or ion gyroradii) have been identified as the sites of important dynamical phenomena in space plasmas. Recent space observations established that thin current sheets often have a bifurcated (double-peaked) current density. Earlier suggestions of possible bifurcation mechanisms are based on the presence of microfluctuations, magnetic reconnection, or a normal magnetic field component or assumed simplified models of adiabatic dynamics. Despite these efforts, the cause (or causes) of the formation of thin bifurcated current sheets and the conditions under which they form have remained unclear. In this paper, we identify quasisteady compression of a plane, initially wide collisionless current sheet as an effective physical mechanism for the formation of thin bifurcated current sheets. Our main tool is electromagnetic particle simulation. The initial sheet has a singly peaked current and a half-width that is five times larger than the ion inertial length. This sheet is quasisteadily compressed by external forces. A three-scale structure develops and the current bifurcates during compression. It is shown that the bifurcation, pressure anisotropy, and other major properties of the embedded current sheet can be understood in terms of basic physical principles, such as electric field shielding and momentum conservation. Sufficient conditions for bifurcation of symmetric current sheets are presented. They suggest that bifurcation must generally occur by quasisteady compression if the (singly peaked) initial current sheet is sufficiently wide. © 2008 American Institute of Physics. [DOI: 10.1063/1.2907359]

I. INTRODUCTION

Current sheets are widely regarded an important element of dynamical processes in space and astrophysical plasmas. This view is based on *in situ* space observations,¹⁻⁴ on magnetohydrodynamic (MHD) considerations and simulations,⁵⁻¹² and on hybrid^{13,14} and kinetic simulations.¹⁵⁻²⁰ For a comparative simulation study, see Ref. 21. In particular, current sheets that are sufficiently thin have been identified as sites of magnetic reconnection,^{4,6,8,22} which is largely believed to be a central building block of magnetospheric and solar activity (see, for example, Refs. 23 and 24). Recent *in situ* evidence demonstrated magnetic reconnection occurring in the turbulent plasma of the Earth's magnetosheath.²⁵

Recent high-resolution spacecraft observations have revealed that in a substantial fraction of thin current sheet observations, the sheet current is bifurcated in the sense that the current density has more than one, mostly two, pronounced peaks. [Note that this feature is to be distinguished from current sheet bifurcation in the sense of statistical mechanics (see, for example, Ref. 26).] Hoshino *et al.*²⁷ presented evidence for current sheet bifurcation in the distant magnetotail. Asano *et al.*^{28,29} used GEOTAIL data to investigate current sheets that develop in the near-Earth magnetotail during substorm growth phases. Typically, current sheets with the largest current densities were found to be bifurcated. CLUSTER data were used by Runov *et al.*^{30,31} in a similar study of magnetotail current sheets located near 19 Earth-radii geocentric distance. They found bifurcation in 5 of 30 current sheet observations. Also the current sheet in the magnetosheath that was studied in detail by Retinó *et al.*²⁵ shows a

bifurcated structure. In these and further observations, typical scale lengths generally were reported to lie in the range of a few to 10 ion inertial lengths or ion gyroradii (computed with the external magnetic field).

In some of the observations, the bifurcation has been attributed to magnetic reconnection occurring in nearby regions of the current sheet (see, for example, Ref. 27). Also particle simulations of magnetic reconnection typically show this feature downstream of the reconnection site.^{15,17,20} However, there are other cases with no evidence for a direct association with reconnection. For example, Runov *et al.*³¹ classified only one of their five bifurcation cases as resulting from reconnection.

Another possible mechanism is the presence of microturbulence modifying the current profile. For lower-hybrid-drift turbulence, current bifurcation was demonstrated by Daughton *et al.*³² and Ricci *et al.*³³

Quasisteady evolution was suggested as a further bifurcation mechanism by Zelenyi *et al.*³⁴ using a simplified description of adiabatic dynamics. In a detailed later study,³⁵ a magnetic field component normal to the current sheet was incorporated.

Despite these results, the process that forms thin current sheets embedded in wider sheets and the conditions under which the current becomes bifurcated have remained largely unclear. It is the aim of this paper to tackle these questions on the basis of an electromagnetic collisionless particle simulation. We will demonstrate that quasisteady compression of a plane sheet, which is wide initially, leads to both features, an embedded current structure on ion and electron

scales and current bifurcation. Neither reconnection nor turbulence nor a normal magnetic field component are required. We isolate the present scenario from others by keeping the sheet strictly one-dimensional spatially; all three velocity components are taken into account.

In this paper, we opted for a thorough discussion of a single simulation. This allowed us to identify the main reasons for the formation of bifurcated thin current sheets by quasistationary compression. These results in turn led to a theoretical analysis resulting in bifurcation criteria valid for much wider choices of parameter sets than could have been covered by further simulations without severely exceeding the scope of this paper.

II. SIMULATION MODEL AND INITIAL CONDITION

Dimensionless quantities are employed throughout the analysis. Densities are normalized by a typical density \tilde{n} in the current sheet, the magnetic field by its initial asymptotic value \tilde{B} . Ions are assumed to be protons (mass $m_i=m_p$) throughout, and the length scale is the ion inertial length c/ω_i , with $\omega_i=\sqrt{e^2\tilde{n}/\epsilon_0m_p}$ the ion plasma frequency evaluated for the reference density. Velocities are measured in units of the ion Alfvén velocity $v_A=\tilde{B}/\sqrt{\mu_0m_p\tilde{n}}$ based on the reference magnitudes of magnetic field and density. The electric field unit is $\tilde{E}=v_A\tilde{B}$, the pressure is measured by units of $\tilde{p}=\tilde{B}^2/\mu_0$, and the current density is normalized by $\tilde{J}=\omega_i\tilde{B}/c\mu_0$. The time unit is the Alfvén time c/ω_iv_A , which coincides with the ion gyrotime $m_p/e\tilde{B}$.

The initial magnetic field is chosen as a Harris sheet.³⁶ It has an x component only, which is of the form

$$B_{x0} = \tanh\left(\frac{z}{5}\right), \quad (1)$$

implying an initial current sheet half-thickness of five ion inertial lengths. For each species s the initial pressure tensor is isotropic and has diagonal components p_{0s} . The ion-electron mass ratio is chosen as $m_i/m_e=25$, the temperature ratio is $T_i/T_e=5$, and v_A/c is set to 0.1. A total of 2.5×10^7 macroparticles are employed in the calculation.

The system evolution is modeled by a (spatially) one-dimensional version of our particle-in-cell code.¹⁷ Particle orbits are calculated in the electromagnetic fields, and the electromagnetic fields are integrated by an implicit method on a grid composed of 2000 cells in the z directions. Driving boundary conditions are employed symmetrically at the upper and lower boundaries located at $z=\pm 40$, in a manner similar to that used by Birn and Hesse.³⁷ The electric field profile is shown in Fig. 1. It leads to a compression along the z axis. The simulation is run until $t=400$, corresponding to 40000 time steps, in order to achieve sufficient relaxation into a new equilibrium. No smoothing is applied within the model or to the results; however, in order to reduce noise, the code output is averaged over $40/\omega_e$, centered at the time of interest.

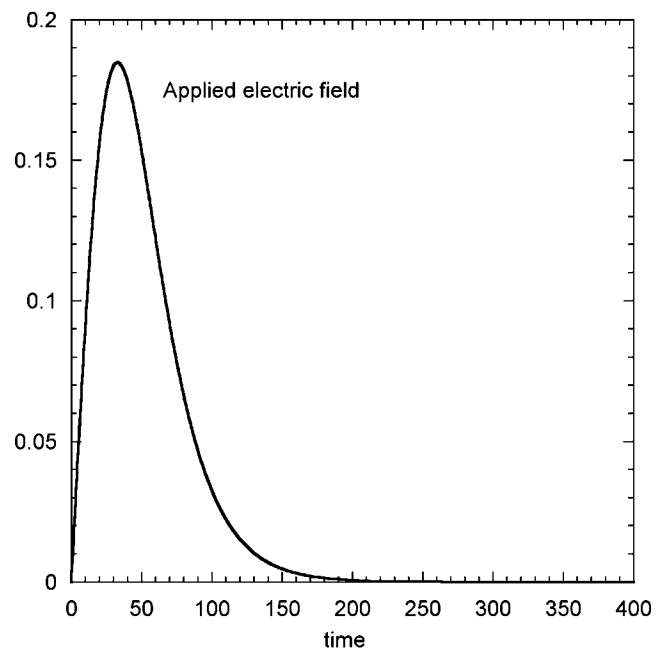


FIG. 1. Time profile of the driving electric field.

III. RESULTS AND INTERPRETATION

Figure 2 shows several quantities initially (thin lines) and after 400 Alfvén times (thick lines). Plotted are the magnetic field component B_x , the pressure tensor component p_{zz} (sum of ion and electron contributions), and the total pressure $p_{tot}=B_x^2/2+p_{zz}$. The compression is manifested by the increase of gradients and of the maximum values of B_x and p_{zz} and of the total pressure. The asymptotic magnetic field magnitude has increased by a factor of 1.3. The compression

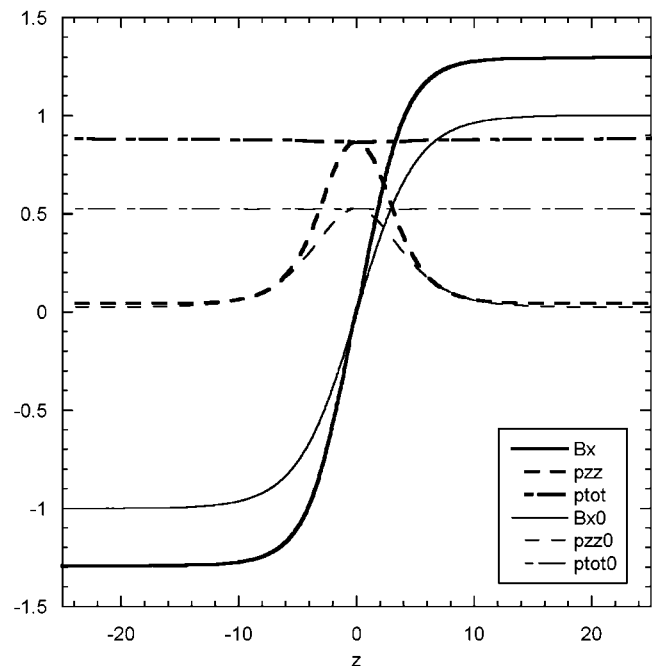


FIG. 2. Shown are B_x , p_{zz} , and p_{tot} vs z initially (thin lines) and after 400 Alfvén times (thick lines).

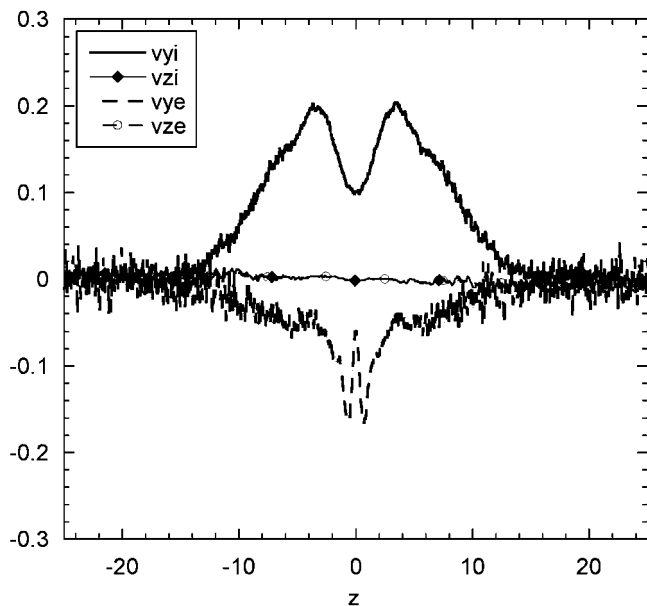


FIG. 3. Ion and electron bulk velocity components after 400 Alfvén times.

is slow and can be approximated by a sequence of quasiequilibrium states. This is indicated by the (approximate) constancy of p_{tot} and the smallness of the z component of the ion and electron velocities (Fig. 3). The components v_{yi} and v_{ye} show double-peaks, which leads to a corresponding bifurcation of the y component of total electric current density J_y (Fig. 4). The other components of the current density are negligibly small.

Another characteristic feature is pressure anisotropy. Figure 5 gives the diagonal components of the ion and electron pressure tensors (full lines). The presence of significant anisotropies is obvious. The nondiagonal components (not shown) are much smaller than the diagonal components and

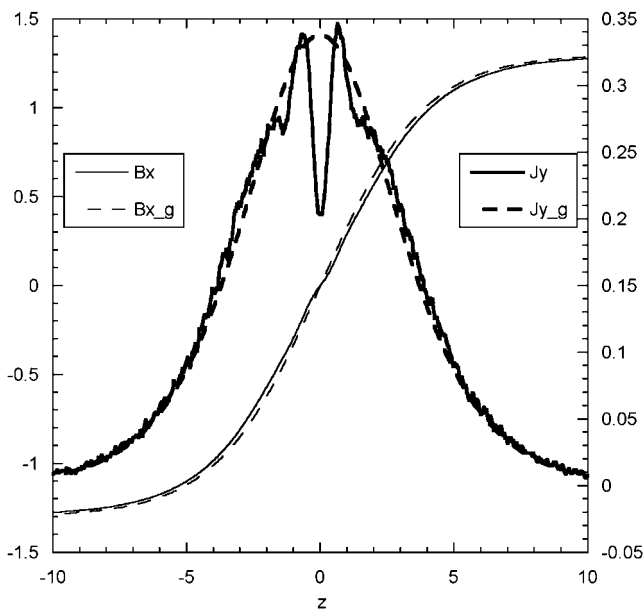


FIG. 4. The electric current density J_y and the magnetic field B_x after 400 Alfvén times and the corresponding gyrotropic model curves.

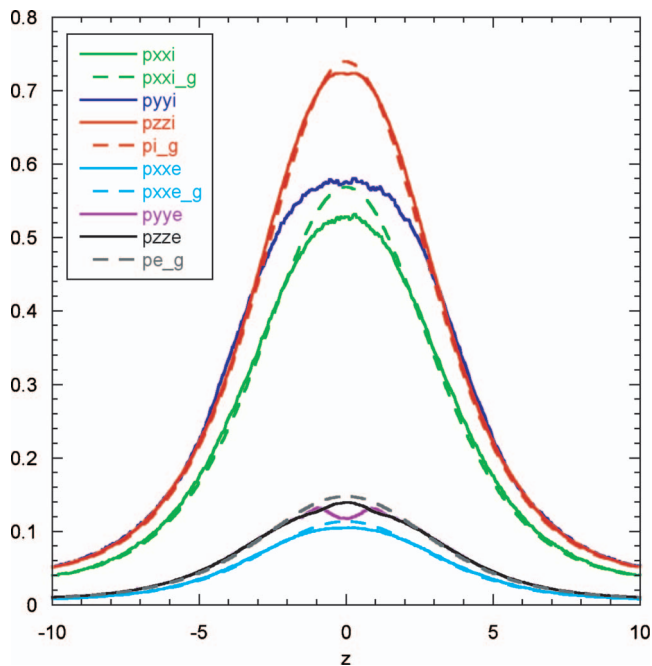


FIG. 5. (Color) The ion and electron pressure tensors (full lines) after 400 Alfvén times and the corresponding gyrotropic model curves (broken lines).

we will ignore them from here on. The current sheet shows three distinctly different regions: a gyrotropic external region and nongyrotropic ion and electron regions, as described below. Although a similar triple structure arises in magnetic reconnection processes (see, for example, Ref. 17), it should be noted that in our case the ion and electron regions do not play the role of diffusion regions.

A. The gyrotropic region

Sufficiently far away from the center ($z=0$), we can expect the plasma to be approximately gyrotropic. The (nondimensional) initial thermal ion gyroradius in the asymptotic magnetic field is 0.91, while the scale length of the initial equilibrium is 5. This suggests the following approximate picture. For each species s , the gyration conserves the pressure tensor isotropy perpendicular to the magnetic field, such that $p_{yys} = p_{zzs}$. Further, for each species the particle number and the magnetic moment are conserved in each flux tube. As there is no compression in the x direction, p_{xxs} scales as the density. This implies the following gyrotropic model:

$$B^g(z) = bB_{x0}(bz), \tag{2}$$

$$n^g(z) = bn_0(bz), \tag{3}$$

$$p_{xxs}^g(z) = bp_{0s}(bz), \tag{4}$$

$$p_{yys}^g(z) = p_{zzs}^g(z) = b^2p_{0s}(bz), \tag{5}$$

$$J_{ys}^g(z) = b^2J_{y0s}(bz), \tag{6}$$

where the superscript g stands for *gyrotropic* and b denotes the relative increase of the magnetic field strength at the boundary by external action, $b = B_x(z_b)/B_{x0}(z_b)$, with z_b being

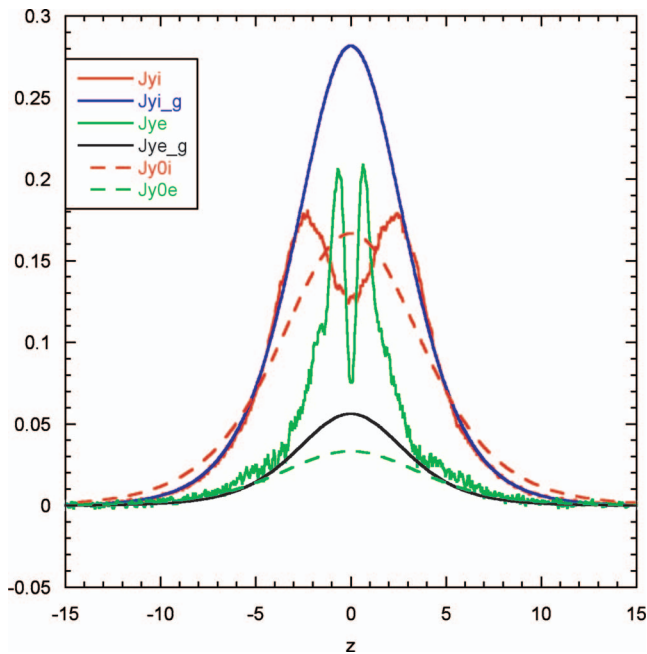


FIG. 6. (Color) The ion and electron current densities initially (broken lines) and after 400 Alfvén times and the corresponding gyrotropic model curves (full lines).

the (positive) location of the boundary. Total pressures and current density are given by the sums of the ion and electron contributions, for example $J_y^g = J_{yi}^g + J_{ye}^g$. The initial quantities are specified in Sec. II. The pressure law (5) can be understood as an adiabatic fluid compression with two degrees of freedom, corresponding to an adiabatic index $\gamma=2$, while Eq. (4) describes isothermal conditions ($\gamma=1$). Figures 4–6 show that for sufficiently large $|z|$, the actual quantities are indeed reasonably approximated by the gyrotropic model expressions (2)–(6) evaluated with the present value $b=1.3$.

B. The ion and electron regions

Figures 4–6 indicate a rather rapid transition from the gyrotropic regime to a different regime, where deviations from the gyrotropic model occur. (B_x shows a less pronounced transition, because the change is in the slope.) A significant ion in-plane anisotropy ($p_{yyi} \neq p_{zzi}$) occurs in $|z| \leq z^* \approx 3$. We expect that z^* can roughly be identified with the thermal ion bounce half-width d_i , which from the simulation, including the effect of the electric field, is obtained as 2.6. (The bounce half-width is the one-sided maximum excursion along z of a thermal particle with vanishing y component of the canonical momentum, i.e., the orbit is centered at the origin.)

There is a corresponding electron region. Its boundary is located near $|z|=0.8$, in good agreement with the electron bounce half-width $d_e=0.84$.

In both cases, the scale is considerably larger than the corresponding inertial scale, which is $c/\omega_{pi}=0.89$ and $c/\omega_{pe}=0.18$. Therefore, we suggest that z^* is determined by ion bouncing. As expected, in the ion region there is an electric field E_z (Fig. 7) that exerts an inward-directed force on the ions, which is necessary for quasineutrality to be main-

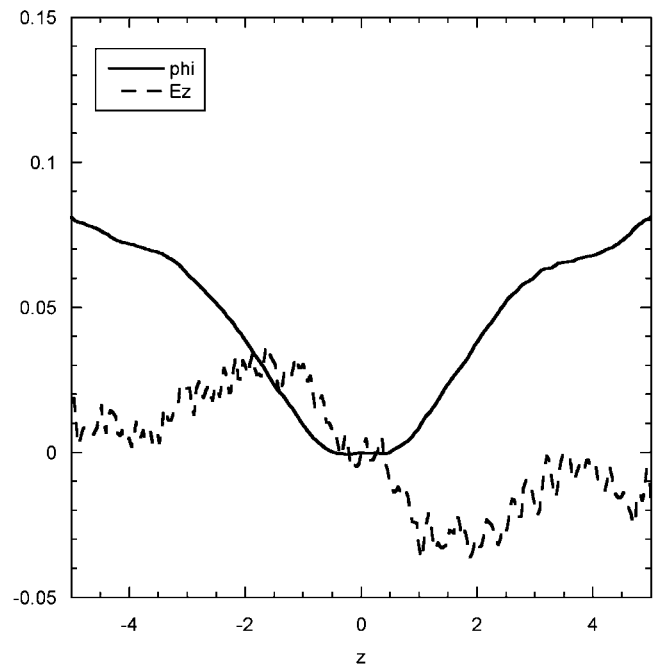


FIG. 7. The electric field component E_z and the corresponding potential ϕ after 400 Alfvén times. The smoothness of the potential curve is due to the numerical integration alone; there is no additional smoothing.

tained. This electric field gives rise to Hall currents, to be discussed further below. The electric field E_z smoothly continues into the electron region before it suddenly decreases to virtually zero, so that there is a small but finite region where the electric field becomes negligibly small. We interpret this effect as electric shielding in a subregion of the electron region where both particle species are unmagnetized and not subject to additional forces. Electron shielding effects have been observed in several previous simulations as well.¹⁷

C. Current bifurcation

A major feature brought out by the present simulation is current bifurcation, which is seen in the total current density (Fig. 8) but also in the ion and electron current densities separately (Fig. 6). We now demonstrate that total current bifurcation can be understood as an immediate consequence of electric field shielding, while ion current bifurcation is directly related to momentum conservation. For dealing with the total current density J_y , let us assume that the electron region not only shields E_z but also the E_y component associated with the temporal evolution. As that evolution is kept rather slow, E_y is very small so that the simulation does not give reliable values. But we can easily test that assumption because it would mean that in the shielding region the magnetic field component B_x must remain unchanged. That this is the case is shown in Fig. 9. Near the origin, the magnetic field B_x closely coincides with the initial field. The shielding causes the slopes of B_x and B_{0x} to agree at the origin. Therefore, the corresponding current densities must also be equal at the origin:

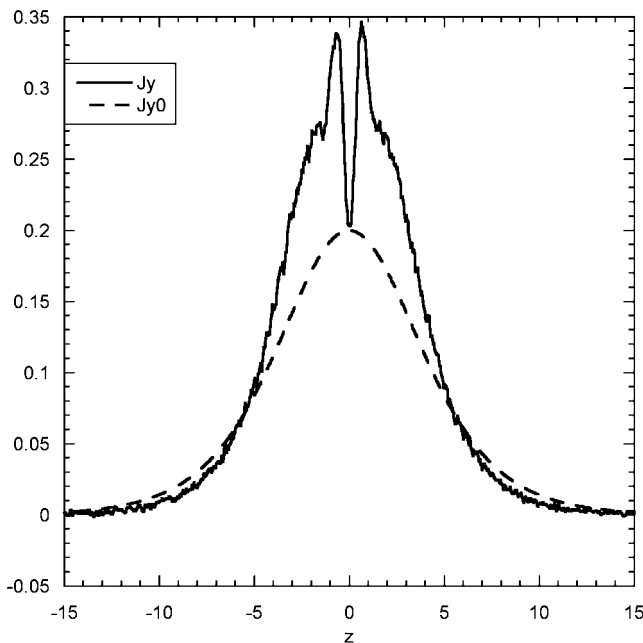


FIG. 8. The electric current density initially and after 400 Alfvén times.

$$J_y(0) = J_{y0}(0). \quad (7)$$

This feature is seen in Fig. 8. As due to the compression the current density has increased substantially above $J_{y0}(0)$ just outside the ion region, there must be a sharp dip of J_y to reach its initial value at the origin. This explains bifurcation of the total current density. Note that the current peaks cannot lie outside the ion region as the initial current density and therefore the gyrotropic approximation (6) vary monotonically in each half-space.

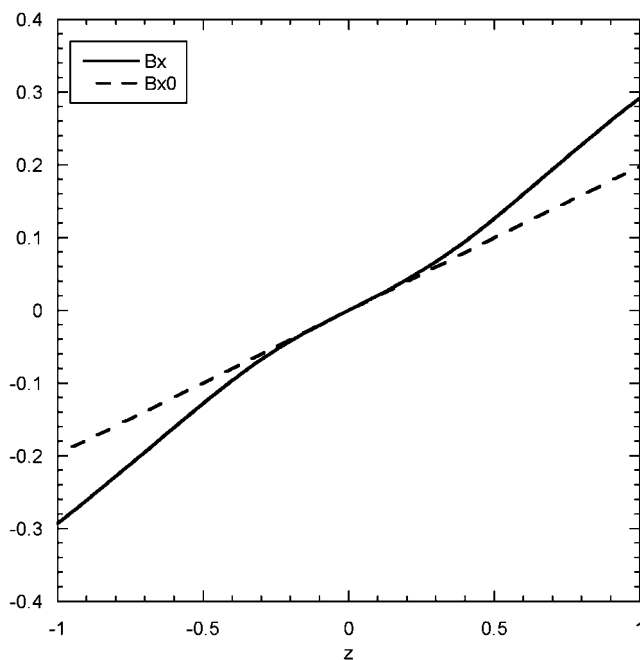


FIG. 9. The magnetic field component B_x initially and after 400 Alfvén times.

Let us now turn to the ion current bifurcation. Hesse *et al.*³⁸ have shown that for a Vlasov plasma consisting of electrons and singly charged ions, global momentum balance can be expressed in the form

$$\frac{d}{dt} \int_V dV \mathbf{J}_i = \frac{m_i}{m_e + m_i} \left(\frac{m_e d\mathbf{I}}{m_i dt} + e\mathbf{M} \right), \quad (8)$$

$$\frac{d}{dt} \int_V dV \mathbf{J}_e = \frac{m_i}{m_e + m_i} \left(\frac{d\mathbf{I}}{dt} - e\mathbf{M} \right), \quad (9)$$

where \mathbf{M} is the momentum flux through the boundary of the domain V and \mathbf{I} is the integrated current

$$\mathbf{I} = \int_V dV \mathbf{J}. \quad (10)$$

In the present case, \mathbf{M} vanishes, because the contributions to the surface integral either cancel by symmetry (with respect to z dependence) or vanish because of vanishing current density. Carrying out the time integration and neglecting the electron mass compared with the ion mass, we find from the y component of Eq. (8)

$$\int_0^{z_b} J_{yi} dz = \int_0^{z_b} J_{y0i} dz, \quad (11)$$

where z_b is the boundary location, which can be replaced by infinity because of the rapid decrease of the integrands for large z . [In this approximation, Eq. (9) is satisfied identically.] Equation (11) means that in Fig. 6, the area under the full and broken red curves must be approximately equal. This is the case within an error near 1%. As the equality of the areas is not reached in the external region (there the area below the full red curve is considerably larger than the area below the broken red curve), this condition requires a considerable reduction of the J_{yi} curve inside the ion region. Note that at the center J_{yi} dips below J_{y0i} to satisfy Eq. (11). This explains the pronounced dip in the ion current density and thereby its bifurcation. Again, the ion current bifurcation structure is thin, because it is within the ion region.

Equation (11) implies further that any increase of the integrated current due to the compression must be carried by the electrons.³⁸ This is consistent with the large peaks of the electron current density in Fig. 6. As in the case of the total current density, the electron current bifurcation can be directly related to the effect of electric shielding. In the ion region, the electron current is dominated by the electron Hall current density $-enE_z/B_x$ (Fig. 10). The shielding effect as discussed above implies that $dE_z/dz=0$ at the origin so that the Hall current vanishes there. This causes two pronounced maxima in the electron Hall current, which becomes the dominant feature of the electron current. To suppress unphysical excursions in the small magnetic field region near the origin, the Hall curve in Fig. 10 has been modified by artificially setting the Hall current density to zero for $|z| < 0.5$. This is motivated by the smallness of E_z (on average) in that region and the corresponding flatness of the potential; both features are evident in Fig. 7.

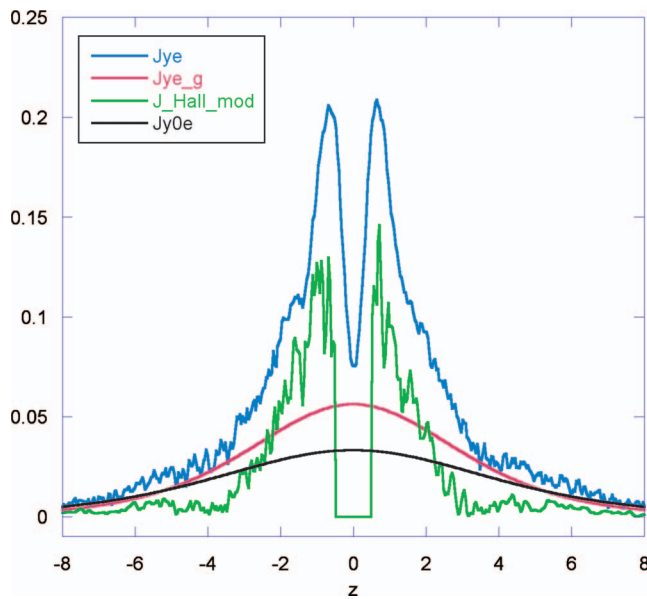


FIG. 10. (Color) Shown are the electron current density after 400 Alfvén times (J_{ye}), its corresponding gyrotropic model curve (J_{ye}^g), the electron Hall current density (J_{Hall}^{mod}), modified as explained in the text, and the initial electron current density (J_{y0e}).

At the center the electron current density stays above its initial value (Fig. 6). This can be understood from Eq. (7) together with the fact that $J_{yi} < J_{y0i}$, as discussed above.

The bifurcation of J_y and J_{yi} can also be understood from a more general point of view. This is shown in the Appendix, where sufficient criteria for current bifurcation are derived. The bottom line is that under rather general conditions, current bifurcation will develop as a result of (quasisteady) compression of a sufficiently wide sheet with an initial singly peaked current density.

D. Pressure tensors

Here we show that several qualitative features of the pressure tensor components can also be understood by properties of the moment equations.

One remarkable feature is the flat top of the ion pressure tensor component p_{zzi} in Fig. 5. The curvature of the curve $p_{zzi}(z)$ at $z=0$ is even smaller than the corresponding initial curvature. This feature is directly related to the ion current bifurcation. To see this, we start from the ion momentum balance

$$-p'_{zzi} + enE_z - J_{yi}B_x = 0, \quad (12)$$

where the prime indicates differentiation with respect to z . Evaluating the derivative of that equation at $z=0$ and, in view of electric shielding, setting E_z and its derivative to zero at the origin, we obtain

$$p''_{zzi}(0) = -J_{yi}(0)J_{y0}(0), \quad (13)$$

where we have replaced the derivative of B_x by the current density and used the property (7). Dividing Eq. (13) by the corresponding equation for the initial state gives

$$\frac{p''_{zzi}(0)}{p''_{zzi}(0)} = \frac{J_{yi}(0)}{J_{y0i}(0)}. \quad (14)$$

Since, as we have seen, the ion bifurcation dip brings the ion current density below its initial value at the origin, the second derivative of p_{zzi} at $z=0$ becomes smaller than the corresponding initial quantity. This explains the flat top of p_{zzi} in Fig. 5. There is no corresponding flattening for the electrons because, at the origin, the electron current density stays above its initial value so that the central curvature of p_{zze} increases compared with the initial curvature.

Another interesting aspect concerns pressure anisotropy. Specializing the Vlasov moment equation for the pressure tensor (see, for example, Ref. 20) for the present quasisteady state conditions and assuming negligible heat flux, we find

$$\frac{p_{zz} - p_{yy}}{p_{zz}} = \pm \frac{1}{B_x} \frac{dv_y}{dz}, \quad (15)$$

where the plus (minus) sign corresponds to the ions (electrons). So, for each species the pressure anisotropy is directly related to the gradient of the bulk velocity. The ion bulk velocity has a dip that is associated with the dip of the ion current density. (The density does not show a dip.) The corresponding derivative dv_{yi}/dz is positive for $z > 0$ and its effect is enhanced near the origin because of B_x becoming small. The result is the ion anisotropy as shown in Fig. 5. A corresponding argument holds for the electrons.

IV. SUMMARY AND DISCUSSION

In this paper, we have investigated the quasisteady compression of an initially wide current sheet in the collisionless plasma regime. We presented results from an electromagnetic particle simulation of a plane configuration. The current sheet, that initially had a Harris-sheet profile of half-width $5c/\omega_{pi}$, developed a thin bifurcated current structure embedded in the wide sheet. Thus, our results established quasisteady compression as an efficient mechanism for the formation of thin bifurcated current sheets.

For our detailed analysis, we chose a relaxed state as it had developed after 400 Alfvén times. The compressed current sheet showed three regions with distinctly different properties. We identify these regions as the gyrotropic or external region, the nongyrotropic ion region, and the nongyrotropic electron region with widths that are in reasonable agreement with the corresponding bounce widths.

The double-peak structure of the current density is confined to the ion region. In that sense, a thin embedded current sheet has formed. Besides the bifurcation, we regard this property as an important result also.

We have interpreted the simulation results with the aid of Vlasov moment equations. We found that a single-scale compression would be inconsistent with momentum conservation, so that an embedded separate structure must necessarily develop. The bifurcation of the total current density can be seen as an immediate consequence of electric field shielding occurring inside the electron region. The ion current bifurcation is best understood as a consequence of momentum conservation. Due to the electric shielding, the electron Hall cur-

rent develops two sharp peaks that exceed the ion current density. For total and ion current bifurcation, criteria were derived in the Appendix. The pressure anisotropy in the v_y , v_z plane can be linked to the derivative of the bulk velocities of the electrons and ions associated with the bifurcation of the current density. The flat top of the ion pressure p_{zzi} is also immediately related to ion bifurcation.

The topic of stability is beyond the scope of this paper. Here we only remark that we expect that bifurcation has a stabilizing effect, while the anisotropy might be destabilizing. This expectation is based on recent results by Matsui and Daughton.³⁹ For postulated equilibria, they found stabilization by bifurcation and destabilization by anisotropy in the regime where the perpendicular (with respect to the magnetic field) electron pressure exceeds the parallel electron pressure, with gyroviscosity also taken into account.

Our results suggest that the physical scale of the kinetic substructure is the ion bounce width rather than the ion inertial scale. Although these scales are not vastly separate in our simulation, nor in many space applications, they may differ significantly in other cases. For illustration consider a Harris sheet, where the bounce width is given by $\sqrt{2La}$, where L is the scale of the sheet and a is the asymptotic gyroradius. Although a equals c/ω_{pi} in this case, for sufficiently large L the ion bounce width can become large compared with the ion inertial length.

The aim of this paper was to establish a basic mechanism for the formation of thin bifurcated current sheets. A simple configuration was chosen in order to keep the physics transparent. We do not expect that our model reproduces observed current sheets in any quantitative details. Nevertheless, it seems instructive to compare a few observed qualitative properties with our simulation results. For bifurcated current sheets, Runov *et al.*³¹ gave details of the number density, the ion temperature, and the sum of magnetic and ion pressure (their Fig. 6). Of these quantities, only the current density shows pronounced double peaks. This is consistent with our simulation results if we identify their ion pressure with p_{zzi} . For instance, Fig. 6 shows pronounced ion current bifurcation, while the ion pressure remains single-peaked (Fig. 5). We also find single peaks for the density and for $B^2/2 + p_{zzi}$. Another property emphasized by Runov *et al.*³¹ is the local dominance of the electron current density; our simulation indeed shows such a dominance at the electron current density peaks (Fig. 6). Concerning the pressure anisotropy, the situation is less clear. Asano *et al.*⁴⁰ and Runov *et al.*³¹ included a statistical analysis of pressure anisotropy, but they only distinguished between pressures parallel and perpendicular to the magnetic field, so that there is no information on the in-plane anisotropy, which plays an important role in our simulation. Asano *et al.*⁴⁰ found cases with the parallel pressure exceeding the perpendicular pressure, but they are not preferred statistically. Further observations with improved time resolution seem necessary to clarify the role of pressure anisotropy. Our results on the role of the Hall current and, particularly, its contribution to the electron current is in line with the view of all authors that we have mentioned regarding this effect as well as others.

Our results clearly exhibit the limitations of the Harris

sheet model, which has been used in many investigations. We have demonstrated that under fairly general conditions, an initial wide Harris sheet that is forced into a phase of quasisteady compression develops several non-Harris features. In particular, a thin subregion arises with structures on the ion and electron scales. In that subregion, the current density becomes bifurcated, the pressure tensor develops a significant anisotropy, and a Hall electric field occurs that cannot be transformed away by a Galilean transformation. In contrast to these complicated kinetic effects appearing in the ion and electron regions, the response of the external region remains simple and can be understood in terms of a gyroviscous model. Also, we have shown that the formation of thin current sheets accompanied by significant Hall electric fields as previously found in two-dimensional configurations^{14,16,18,19,21} is a fundamental process and does not require a second spatial dimension.

Several extensions of this work are desirable. In particular, this applies to exploring nonsymmetric configurations, to admitting a second spatial dimension allowing for a normal magnetic field component, and to investigating stability.

ACKNOWLEDGMENTS

One of us (K.S.) gratefully acknowledges the kind hospitality he enjoyed at the Goddard Space Flight Center during a visit in the fall of 2007. M.H.'s contribution to this work was supported by NASA's Magnetospheric Multiscale Mission. We thank Joachim Birn, William Daughton, and Jürgen Dreher for helpful remarks and comments.

APPENDIX: BIFURCATION CRITERIA

Here we derive sufficient criteria for bifurcation expressed by properties of the initial configuration and the electron and ion bounce widths $d_e < d_i$, which we assume to represent the widths of the ion and electron region, respectively.

First let us consider the total current density $J_y(z)$. We assume quasistationary compression of a one-dimensional Vlasov plasma with the same coordinate orientation, symmetry, and composition as in the present simulation. Initially, the current density uniformly approaches zero for sufficiently large $|z|$, so that J_{y0} becomes negligible at the boundary, which for simplicity is placed at infinity, the integrated current remaining finite. Further, J_{y0} has a single extremum, which by symmetry is located at $z=0$. Without loss of generality, we assume that J_{y0} is positive (Fig. 11). The instantaneous enhancement factor of the asymptotic magnetic field is $b > 0$. Based on properties of the simulation, we also assume that J_y can be approximated by J_y^g [as defined in Eq. (6) for each species] outside the ion region and that there is electric field shielding in a finite region lying inside the electron region.

Let $z_c > 0$ be a critical location defined by the solution of the equation

$$J_y^g(z_c) = J_{y0}(0). \quad (\text{A1})$$

Note that Eq. (A1) has a unique positive solution.

Under these conditions, the following bifurcation criterion holds: If

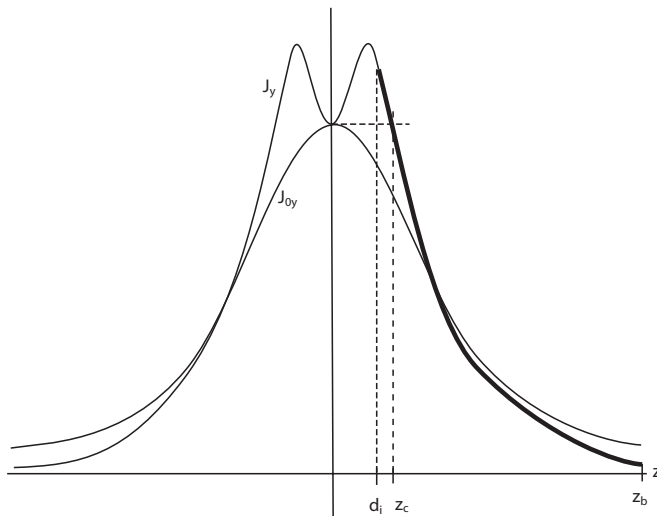


FIG. 11. Sketch on the bifurcation criterion for the total current density.

$$d_i < z_c, \quad (\text{A2})$$

the current density J_y has at least two maxima in the region $|z| < d_i$.

The proof of this criterion is straightforward. The assumptions and the condition $d_i < z_c$ imply that $J_y(d_i) > J_{y0}(0)$, see Fig. 11. Note that necessarily $J_y(z)$ is monotonic in $z > d_i$ (thick line in Fig. 11), as a consequence of the monotonicity of J_{y0} carried over to J_y^g . By electric shielding, we have $J_y(0) = J_{y0}(0)$. Thus, continuity requires that there must exist at least one maximum of J_y in $z > 0$. Because of the external monotonicity of J_y , that maximum must be located in $0 < z < d_i$. Symmetry then ensures that there exist at least two maxima in $-d_i < z < d_i$, which concludes the proof.

A similar criterion holds for bifurcation of the ion current density. Imposing on J_{y0i} the same properties that were formulated above for J_{y0} , let us define z_{ci} by

$$J_{yi}^g(z_{ci}) = J_{y0i}(0). \quad (\text{A3})$$

The electric field shielding property is replaced by the momentum balance condition (11). Then the ion bifurcation criterion is obtained in the following form: If

$$d_i < z_{ci} \quad (\text{A4})$$

and

$$\int_{d_i}^{\infty} [J_{yi}^g(z) - J_{y0i}(z)] dz > 0, \quad (\text{A5})$$

the current density J_y has at least two maxima in the region $|z| < d_i$.

First we note that both conditions are satisfied for sufficiently small d_i . For the second condition, this is easily verified by noting that for $d_i \rightarrow 0$ the integral becomes $(b-1) \int_0^{\infty} J_{y0i}(z) dz > 0$.

Similar to the procedure described above for bifurcation of the total current density, we conclude from $d_i < z_{ci}$ that $J_{yi}(d_i) > J_{y0i}(0)$. Momentum balance (11) together with Eq. (A5) gives

$$\int_0^{d_i} [J_{yi}(z) - J_{y0}(z)] dz < 0. \quad (\text{A6})$$

This means that in $(0, d_i)$ there exists a point \hat{z} , such that $J_{yi}(\hat{z}) < J_{y0i}(\hat{z})$. Taking into account the assumption $d_i < z_{ci}$ and monotonicity of J_{y0i} for $z > 0$, we can conclude from Eq. (A6) that $J_{yi}(\hat{z}) < J_{yi}(d_i)$, which implies at least one maximum in $0 < z < d_i$. Again, by symmetry, a second maximum exists for negative z , which proves the criterion.

For the present simulation, the conditions (A2), (A4), and (A5) are fulfilled.

As the criteria derived above require the knowledge of d_i , it is desirable to formulate the criteria in terms of initial quantities alone. Fortunately, if the conditions (A2), (A4), and (A5) are satisfied originally, they are satisfied in any compressed state, as long as the compression does not decrease the magnetic field strength near the origin and E_z , which also influences d_i , is negative so that the ions are pulled toward the center. These are features of the present simulation and should hold quite generally for current sheets with the properties specified above.

- ¹R. L. Kaufmann, *J. Geophys. Res.* **92**, 7471, DOI: 10.1029/JA092iA07p07471 (1987).
- ²D. G. Mitchell, D. J. Williams, C. Y. Huang, L. A. Frank, and C. T. Russell, *Geophys. Res. Lett.* **17**, 583, DOI: 10.1029/GL017i005p00583 (1990).
- ³V. A. Sergeev, P. Tanskanen, K. Mursula, A. Korth, and R. C. Elphic, *J. Geophys. Res.* **95**, 3819, DOI: 10.1029/JA095iA04p03819 (1990).
- ⁴T. I. Pulkkinen, D. N. Baker, D. G. Mitchell, R. L. McPherron, C. Y. Huang, and L. A. Frank, *J. Geophys. Res.* **99**, 5793, DOI: 10.1029/93JA03234 (1994).
- ⁵E. N. Parker, *Astrophys. J.* **174**, 499 (1972).
- ⁶E. R. Priest, in *Solar Flare Magnetohydrodynamics*, edited by E. R. Priest (Gordon and Breach, New York, 1981), pp. 139–215.
- ⁷B. C. Low, *Astrophys. J.* **323**, 358 (1987).
- ⁸D. Biskamp, *Phys. Fluids* **29**, 1520 (1986).
- ⁹K. Schindler and J. Birn, *J. Geophys. Res.* **98**, 15477, DOI: 10.1029/93JA01047 (1993).
- ¹⁰E. N. Parker, *Spontaneous Current Sheets in Magnetic Fields: With Applications to Stellar X-rays* (Oxford University Press, New York, 1994).
- ¹¹A. Voge, A. Otto, and K. Schindler, *J. Geophys. Res.* **99**, 21241, DOI: 10.1029/93JA02074 (1994).
- ¹²J. Birn, M. Hesse, and K. Schindler, *J. Geophys. Res.* **103**, 6843, DOI: 10.1029/97JA03602 (1998).
- ¹³M. Hesse, D. Winske, M. Kuznetsova, J. Birn, and K. Schindler, *J. Geomagn. Geoelectr.* **48**, 749 (1996).
- ¹⁴K. Arzner and M. Scholer, *J. Geophys. Res.* **106**, 3827, DOI: 10.1029/2000JA000179 (2001).
- ¹⁵P. L. Pritchett, F. V. Coroniti, R. Pellat, and H. Karimabadi, *J. Geophys. Res.* **96**, 11523, DOI: 10.1029/91JA01094 (1991).
- ¹⁶P. L. Pritchett and F. V. Coroniti, *J. Geophys. Res.* **100**, 23551, DOI: 10.1029/95JA02540 (1995).
- ¹⁷M. Hesse, K. Schindler, J. Birn, and M. Kuznetsova, *Phys. Plasmas* **6**, 1781 (1999).
- ¹⁸P. L. Pritchett, *J. Geophys. Res.* **106**, 25961, DOI: 10.1029/2001JA000016 (2001).
- ¹⁹M. Hoshino, T. Mukai, T. Terawasa, and I. Shinohara, *J. Geophys. Res.* **106**, 25979, DOI: 10.1029/2001JA900052 (2001).
- ²⁰M. Hesse, M. Kuznetsova, and J. Birn, *Phys. Plasmas* **11**, 5387 (2004).
- ²¹J. Birn, K. Galsgaard, M. Hesse, M. Hoshino, J. Huba, G. Lapenta, P. L. Pritchett, K. Schindler, L. Yin, J. Büchner, T. Neukirch, and E. R. Priest, *Geophys. Res. Lett.* **32**, L06105, DOI: 10.1029/2004GL022058 (2005).
- ²²J. Birn and K. Schindler, *J. Geophys. Res.* **107**, 1117, DOI: 10.1029/2001JA000291 (2002).
- ²³E. R. Priest and T. G. Forbes, *Magnetic Reconnection* (Cambridge University Press, Cambridge, UK, 2000).
- ²⁴K. Schindler, *Physics of Space Plasma Activity* (Cambridge University

- Press, Cambridge, UK, 2007).
- ²⁵A. Retinò, D. Sundkvist, A. Vaivads, F. Mozer, M. André, and C. J. Owen, *Nat. Phys.* **3**, 235 (2007).
- ²⁶M. Hesse and K. Schindler, *Phys. Fluids* **29**, 2484 (1986).
- ²⁷M. Hoshino, A. Nishida, T. Mukai, Y. Saito, T. Yamamoto, and S. Kokubun, *J. Geophys. Res.* **101**, 24775, DOI: 10.1029/96JA02313 (1996).
- ²⁸Y. Asano, T. Mukai, M. Hoshino, Y. Saito, H. Hayakawa, and T. Nagai, *J. Geophys. Res.* **109**, A02212, DOI: 10.1029/2003JA010114 (2004).
- ²⁹Y. Asano, R. Nakamura, W. Baumjohann, A. Runov, Z. Vörös, M. Volwerk, T. L. Zhang, A. Balogh, B. Klecker, and H. Rème, *Geophys. Res. Lett.* **32**, L03108, DOI: 10.1029/2004GL021834 (2005).
- ³⁰A. Runov, V. A. Sergeev, R. Nakamura, W. Baumjohann, Z. Vörös, M. Volwerk, Y. Asano, and B. Klecker, *Ann. Geophys.* **24**, 2535 (2004).
- ³¹A. Runov, V. A. Sergeev, R. Nakamura, W. Baumjohann, S. Apatenkov, Y. Asano, T. Takada, M. Volwerk, Z. Vörös, T. L. Zhang, J.-A. Sauvaud, H. Rème, and A. Balogh, *Ann. Geophys.* **24**, 247 (2006).
- ³²W. Daughton, G. Lapenta, and P. Ricci, *Phys. Rev. Lett.* **93**, 105004 (2004).
- ³³P. Ricci, J. U. Brackbill, W. Daughton, and G. Lapenta, *Phys. Plasmas* **12**, 055901 (2005).
- ³⁴L. M. Zelenyi, M. I. Sitnov, H. V. Malova, and A. S. Sharma, *Nonlinear Processes Geophys.* **7**, 127 (2000).
- ³⁵L. M. Zelenyi, H. V. Malova, V. Y. Popov, D. C. Delcourt, and A. S. Sharma, in *Frontiers in Magnetospheric Plasma Physics* (Elsevier, Amsterdam, 2005), pp. 100–107.
- ³⁶E. G. Harris, *Nuovo Cimento* **23**, 115 (1962).
- ³⁷J. Birn and M. Hesse, *Phys. Plasmas* **14**, 082306 (2007).
- ³⁸M. Hesse, D. Winske, and J. Birn, *Phys. Scr., T* **T74**, 63 (1998).
- ³⁹T. Matsui and W. Daughton, *Phys. Plasmas* **15**, 012901 (2008).
- ⁴⁰Y. Asano, T. Mukai, M. Hoshino, Y. Saito, H. Hayakawa, and T. Nagai, *J. Geophys. Res.* **109**, A05213, DOI: 10.1029/2004JA010413 (2004).